Interface mobility and the liquid-glass transition in a one-component system described by an embedded atom method potential

M. I. Mendelev,[1] J. Schmalian,[1,2,3] C. Z. Wang,[1,2] J. R. Morris,[4,5] and K. M. Ho[2,3]
[1]*Materials and Engineering Physics, Ames Laboratory, Ames, Iowa 50011, USA*
[2]*Condensed Matter Physics, Ames Laboratory, Ames, Iowa 50011, USA*
[3]*Department of Physics and Astronomy, Iowa State University, Ames, Iowa 50011, USA*
[4]*Metals and Ceramics Division, Oak Ridge National Laboratory, Oak Ridge, Tennessee 37831, USA*
[5]*Department of Materials Science and Engineering, University of Tennessee, Knoxville, Tennessee 37996, USA*
(Received 19 December 2005; revised manuscript received 9 August 2006; published 29 September 2006)

We present molecular dynamics (MD) studies of the liquid structure, thermodynamics, and dynamics in a one-component system described by the Ercolessi-Adams embedded atom method potential for Al. We find two distinct noncrystalline phases in this system. One of them is a liquid phase and the second phase has similar structure but different equation of state. Moreover, this phase has qualitatively different dynamics than that in the liquid phase. The transitions between these two noncrystalline phases can be seen during MD simulation. The hysteresis in this transition suggests that this is a first-order transition. This conclusion is strongly supported by simulations of the two phases that demonstrate that these phases may coexist with a well-defined interface. We find the coexistent temperature and the interface mobility. Finally, we discuss how these results can be explained using modern models of vitrification.

DOI: 10.1103/PhysRevB.74.104206 PACS number(s): 61.20.Ja, 61.43.Dq, 64.70.Pf, 66.30.Fq

I. INTRODUCTION

Metallic liquids have attracted a lot of attention, both because of various technological applications[1–3] and because of a fundamental interest in the structure, correlations, and dynamics of a strongly interacting many body system.[4] Cooling down a metallic liquid yields a broad spectrum of possible low temperature states, ranging from "ordinary" crystallization into a periodic lattice to the formation of aperiodic quasicrystals[5] or to metallic glasses,[6] usually as a result of a rapid quench of the liquid state. In addition, more exotic Frank-Kaspar phases,[3] with ordered structures of defect lines or points, have been proposed and are closely related to metallic glasses with strong icosahedral short range order.[7] Another option for the system evolution during supercooling is a liquid-liquid transition; this is a first-order phase transition between two distinct liquid phases which recently attracted considerable interest.[8–10]

Experimentally, metallic glass formation from quenched liquids has only been observed in multicomponent systems. A natural explanation for this observation is associated with the necessity of "mass transport" of the different components to form crystal phases. For example, an explanation of the asymmetry of the glassy regions with respect to the eutectic points of two-component systems was recently proposed in Ref. 11 and was demonstrated to be in good agreement with experiment. On the other hand, important insight into the theory of structural glasses was obtained using theories that are based on a single-component approach.[12,13] While it is known that single-component systems, like particles interacting via a Lennard-Jones potential, may crystallize on molecular dynamics (MD) time scales, it is nevertheless unclear whether the difference between single-component and binary Lennard-Jones mixtures is solely quantitative (resulting from limitations in simulation time or length scales) or more fundamental.[14] We further note that there are several known metallic glasses such as ZrCu that form at the same composition as the stable crystal phase, so mass transport is not a necessary condition for forming a metallic glass.

Molecular dynamics simulation is a powerful tool to investigate correlations and dynamics of supercooled liquids. Such simulations of a supercooled atomic liquid consisting of binary Lennard-Jones mixtures revealed a power-law time dependence and temperature dependence of the self-intermediate-scattering function in the β-relaxation regime.[14,15] This behavior is in agreement with the prediction of the mode-coupling theory above a dynamical crossover temperature and thus in full agreement with the behavior of glass formation as described in Refs. 12, 13, and 16–18. In addition, the study of the out-of-equilibrium dynamic correlations showed a strong dependence of the correlation functions on the waiting time, i.e., ageing below the dynamical freezing temperature.[19–21] The fragility, the configurational entropy, and the potential energy landscape in glass-forming systems have been demonstrated to be closely related[22] and distinct dynamical regimes have been observed, as expected from the theories of glass formation based on an entropy crisis approach.[16,23] A close relationship between the energy landscape approach to the glassiness and the unconventional dynamics of the glassy state was demonstrated in Ref. 24.

Molecular dynamics simulations of metallic liquids[25–30] demonstrated that in binary systems the key signatures of vitrification are rather similar to organic glass-forming materials, including detailed comparisons with the mode coupling approach to supercooled liquids.[31] In particular, the comparison between single-component and binary systems made in Ref. 28 as well as the detailed investigation of the competition between nucleation and vitrification in Cu (Ref. 32) revealed that a deeper understanding of the nucle-

ation dynamics in supercooled metallic liquids can be obtained by investigating model systems consisting of one component only.

Thus, a key motivation for this work is to investigate whether glass formation in a single-component system has a similar character to that encountered in structural glasses. In this work, we demonstrate that a commonly used, embedded atom method (EAM) (Ref. 33) interatomic potential for Al (Ref. 34) exhibits a transition to a disordered, metastable low temperature phase, which we shall refer to as the γ phase. This phase forms spontaneously and discontinuously from the liquid phase on cooling. The liquid phase may also be formed by heating the γ phase, at a temperature below the fcc melting temperature. This hysteresis indicates that there may be a first-order phase transition between these noncrystalline phases. In fact, we demonstrate that this transition has all of the hallmarks of a first-order phase transition, including a latent heat and coexistence of phases with a discontinuous phase boundary. We further demonstrate that the interface between them may be driven in either direction by appropriately changing of temperature away from coexistence, allowing us to determine the mobility of the interface.

II. INTERATOMIC POTENTIAL

It was our goal to study the possibility of glass formation in a single-component metal. Therefore, we chose the interatomic potentials of the EAM type. This was motivated by the fact that while EAM potentials are computationally not more expensive than pair potentials, they are capable to reproduce some important metal properties (e.g., the Cauchy pressure[33]), which cannot be in principle done using pair potential. Recall that the total potential energy U, in the embedded atom method framework, has contributions from pairwise and local density terms

$$U = \sum_{i=1}^{N-1} \sum_{j=i+1}^{N} \varphi(r_{ij}) + \sum_{i=1}^{N} \Phi(\rho_i), \tag{1}$$

where the subscripts i and j label distinct atoms, N is the number of atoms in the system, $r_{i,j}$ is the separation between atoms i and j and

$$\rho_i = \sum_j \psi(r_{ij}), \tag{2}$$

where ψ is a spherically symmetric density function density. We considered two EAM potentials developed for Al. The first one was proposed in Ref. 34 (we refer to this potential as EA; the parameters of this potential was taken from Ref. 35) and the second one was developed in Ref. 36 (we refer to this potential as MSAHM). They were both fitted to the atomic forces obtained from first-principles calculations of various liquid configurations as well as to $T=0$ crystal properties and melting point data. Furthermore, they both have melting temperatures within ~1% of the experimental melting temperature of aluminum.

When we simulated the supercooled liquid using the MSAHM potential, we observed at $T=500$ K a sudden change in the pressure and in the mean square displacement

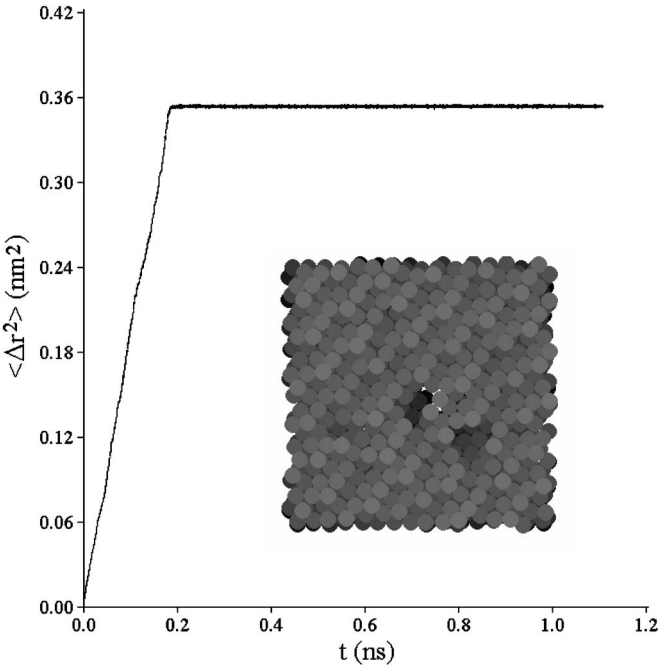

FIG. 1. Mean square displacement for the model created with the MSAHM potential at $T=500$ K and a snapshot of the model after MD relaxation. Two cavities seen in the snapshot are associated with the fact that the simulation was performed in NVT ensemble and the fcc density is essentially larger than the liquid density.

versus time dependence as shown in Fig. 1. Visual analysis together with analysis of pair correlation function (PCF) and angle distributions showed that we observed the solidification into an fcc structure during this MD simulation (see Ref. 37 for details). On the other hand, we never observed such a transition in the EA system, despite many long simulations at different temperatures. This difference between the two potentials can be attributed to the difference in the solid-liquid interface free energy: an accurate MD simulation shows that this value is 1.5 times larger in the EA system.[38] Given that the nucleation barrier scales as the cube of the interfacial free energy, and the nucleation rate is exponentially slow in this quantity, it is reasonable to assume that this prevents solidification in the EA system. However, we believe that there is another mechanism at work: instead of forming the stable fcc crystalline phase from the undercooled liquid, the system forms a noncrystalline solid phase. This phase forms rapidly near $T=600$ K, as we demonstrate later; in comparison, the MSAHM potential does not nucleate the fcc phase until temperatures below this.[37]

Experimentally, vitrification is never observed in pure Al. Therefore, the MSAHM potential is likely more appropriate for studying the solidification in Al. Nevertheless, it is still worth studying the liquid-glass transition using the EA potential in the one-component system to clarify the roles played by two different phenomena which simultaneously occur during vitrification in any multicomponent system: the first is associated with the diffusion of different components and the second one is associated with the necessity to form a glass phase from the liquid. Simulation in a one-component

system will allow us to focus on the second aspect and to demonstrate coexistence between two disordered phases in a single-component system.

The EA potential has been already used to study vitrification.[39,40] The authors of these papers were focused on the dependence of some properties on the cooling rate. They started from $T=1400$ K and cooled the model down to $T=0$. The slowest rate was 1.9×10^{12} K/s. Therefore, the longest total simulation time was 0.73 ns. As it will be shown, below 0.7 ns is the time that is necessary to observe the transition in the MD simulation with the EA potential. Therefore, what the authors of Refs. 39 and 40 observed were probably changes due to the underlying transition discussed in this paper and due to the cooling of the system. In distinction to Refs. 39 and 40, we try to find metastable states at each temperature by equilibrating the simulation cell until the model properties stop changing. Hence, the cooling rate is not used as a parameter in this study.

III. SIMULATION OF LOW AND HIGH TEMPERATURE NONCRYSTALLINE PHASES

A. Creation of atomic models of low and high temperature noncrystalline phases

The main methodological problem of the atomistic simulation of liquid-glass transition is how to clearly distinguish these two noncrystalline phases. Experimentally, the glass transformation is defined either by its viscosity on cooling or by structural relaxation detected by calorimetry on heating from the quenched amorphous phase. Neither of these is practical for the time scales available from simulations. Obviously, the identification of the different phases cannot be done by simple visual analysis of atomic positions as may be done in the case of the liquid-crystal transition. In this section, we describe how we generated two different noncrystalline phases. While we will argue in Sec. VI whether we can really consider the low temperature phase as a glass phase, here we will simply call these phases as liquid and γ.

In order to obtain the liquid, we started from random atomic configuration which was equilibrated at $T=950$ K (the melting temperature for this potential is 925 K; see Sec. V). The model consisted of 2000 atoms in the simulation cell with periodic boundary conditions. The simulation cell size was chosen to provide zero pressure in the NVT (i.e., N=const, V=const, and T=const) molecular dynamics simulation.[41] The model properties were averaged over 2 000 000 MD steps (4.1 ns). Figure 2 shows the pair correlation function of the liquid. The results are typical for single-component metal liquids except for a small asymmetry of the second peak. This feature of the EA potential may be the reason why this potential predicts a large solid-liquid interface free energy.[38] Figure 3 demonstrates that the mean square displacement is a linear function of time. The slope to this curve gives the diffusivity

$$D=\frac{\langle\Delta r^2\rangle}{6t}. \tag{3}$$

The obtained value, 3.7×10^{-5} cm^2 s, is typical for liquid metals near the melting temperature.

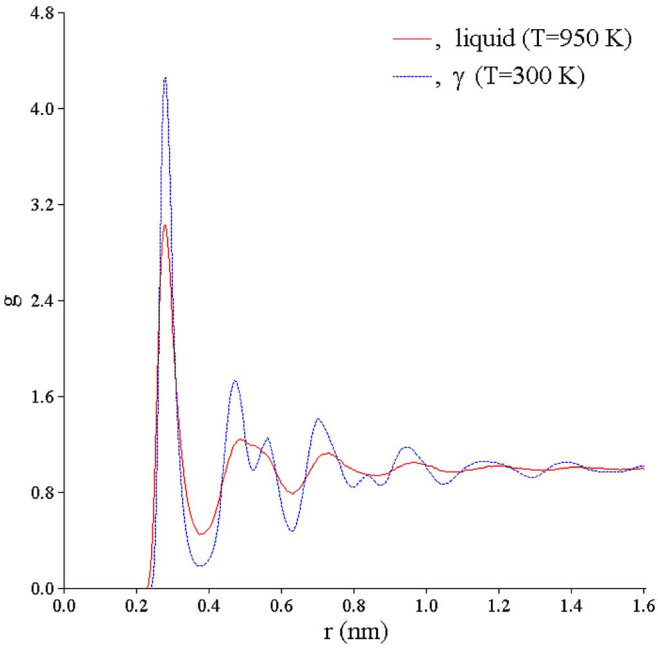

FIG. 2. (Color online) PCFs of the liquid and γ phases.

We then cooled this model down to 300 K, keeping the pressure equal to zero and relaxed it during 10 000 000 MD steps. The PCF and mean square displacement for this structure, which we will call γ phase, are shown in Figs. 2 and 3. The main differences between the PCFs at $T=950$ K and $T=300$ K are the considerable increase of the first peak height, and pronounced splitting of the second peak of the PCF at low temperature. These features are commonly attributed to the amorphous phase.[42] Figure 3 demonstrates that the diffusion is almost absent in the model except for a few isolated jumps.

Next we cooled down the liquid as follows: we instantaneously decreased the temperature by 50–100 K, relaxed the system at constant temperature during 20 000 MD steps and found the equilibrium density by calculation of the pressure for several simulation cell volumes. Then we relaxed the system at the equilibrium density during another 20 000 MD steps and finally averaged its characteristics during 2 000 000 MD steps. The value of the pressure averaged over these 2 000 000 MD steps was less than 0.02 GPa (the pressure mean square fluctuation is 0.097 GPa at $T=950$ K). Figures 4–6 demonstrate the volume, energy, and diffusivity [calculated using Eq. (3)] as functions of temperature. All functions are very smooth. However, when we tried to do such relaxation at $T=550$ K, the system behaved as a liquid during the first 250 000 MD steps (0.5 ns); then suddenly the pressure dropped to −0.87 GPa. Figure 7 demonstrates that at the same time the diffusivity decreased by almost an order of magnitude. These results indicate a transition of the liquid into the γ phase.

We also heated up the γ phase using the same procedure as described above. The only difference was that this time the system required much longer time to equilibrate (we concluded that the system is in metastable equilibrium when the average pressure stopped changing). The data shown in Figs. 4–6 are also averaged over 2 000 000 MD steps. These

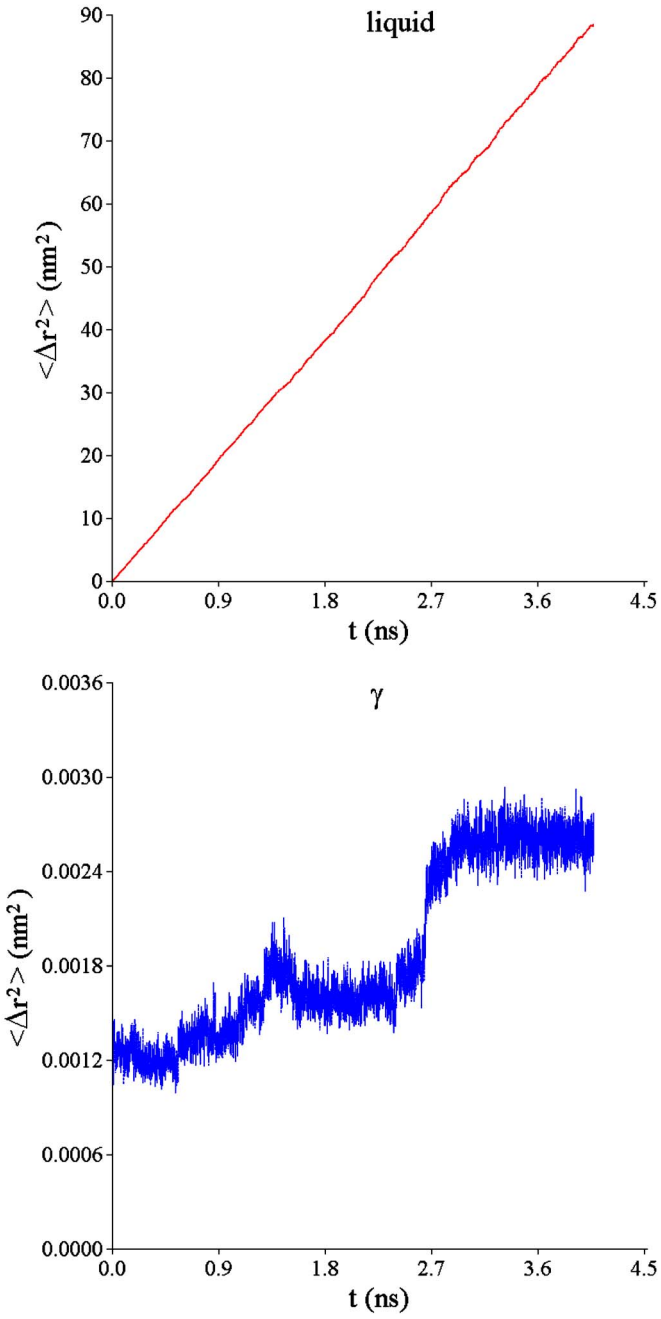

FIG. 3. (Color online) Mean square displacement in the liquid phase at $T=950$ K and in the γ phase at $T=300$ K.

curves are not as smooth as the data for the liquid. This probably means that the system size for the low temperature noncrystalline phase should be larger in order to get better statistics. When we tried to relax the model at $T=830$ K, the pressure was constant during first 500 000 MD steps (0.9 ns), and then increased up to 1.4 GPa. Figure 7 demonstrates that the diffusivity increased by a factor of 5 at the same time. Thus, the γ phase melts around 830 K.

It is important to note that the curves for the liquid and γ phases shown in Figs. 4–6 do not merge and there is a rather large temperature interval where we were able to obtain the properties of both phases. In order to check whether these results are affected by the relatively small size of the system

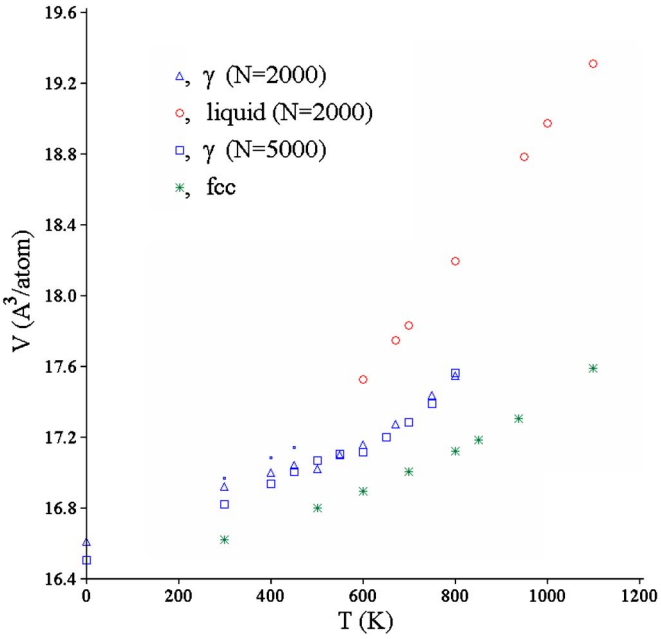

FIG. 4. (Color online) Atomic volume as function of temperature.

(2000 atoms) we repeated all simulations for $N=5000$. Note that the $N=5000$ series was completely independent of the $N=2000$ series. The results are also shown in Figs. 4–6. In the case of the high temperature phase (liquid), we did not find any difference between $N=2000$ and $N=5000$ series. In the case of the low temperature phase (γ), we found that $N=5000$ models require much longer time to equilibrate at very low temperature. When we started from a model at $T=300$ K it was unclear whether the system was indeed equilibrated at this temperature since all atomic processes occurred very slowly. We heated this model up to $T=500$ K (small

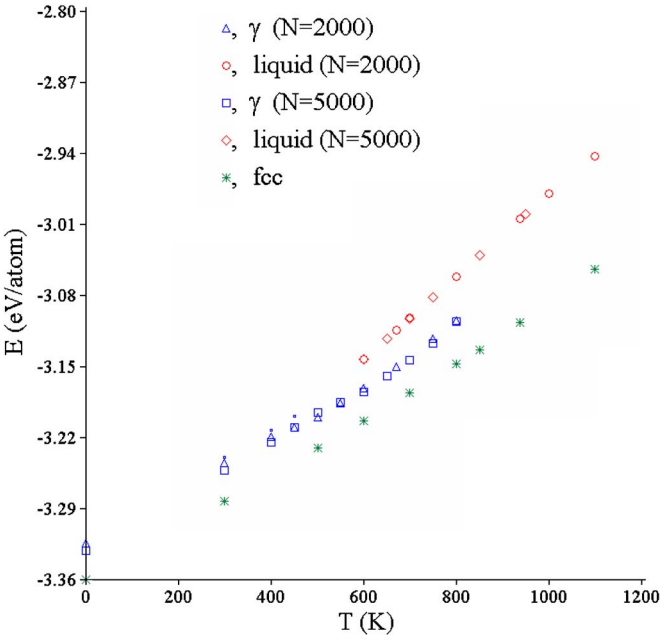

FIG. 5. (Color online) Energy as function of temperature.

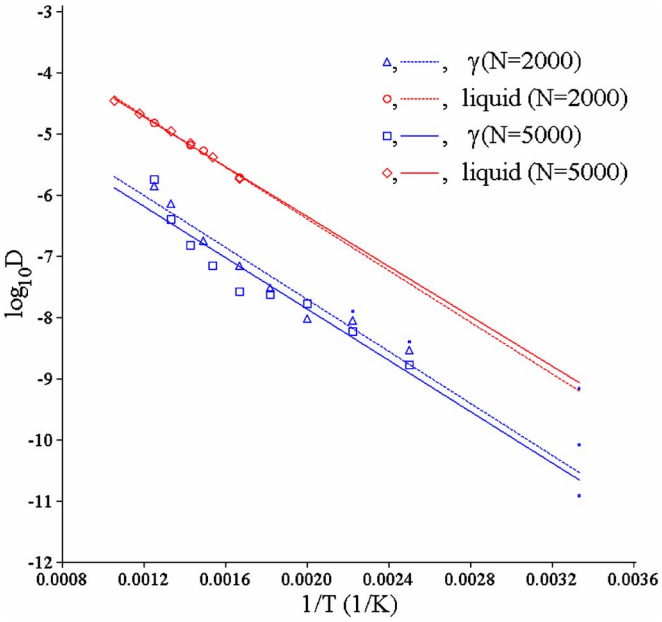

FIG. 6. (Color online) Diffusivity as function of temperature.

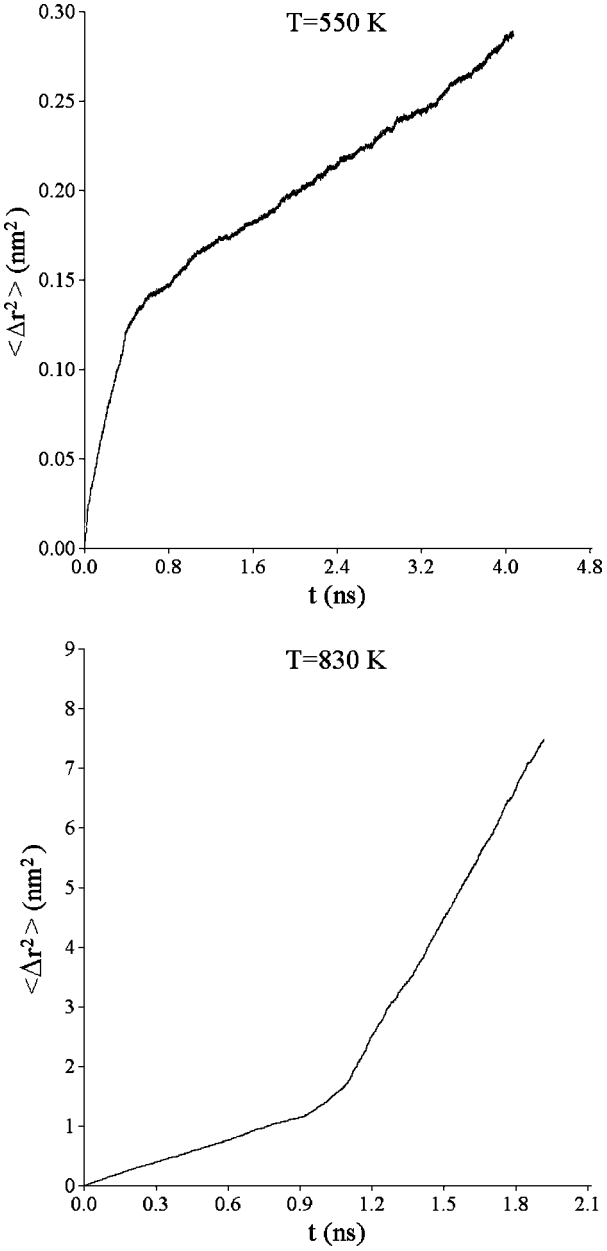

FIG. 7. Mean square displacement in initially liquid phase at $T=550$ K and in initially γ phase at $T=830$ K. The NVT simulation was used in both cases.

squares in Figs. 4–6) and then all data for this series shown in Figs. 4–6 (large squares) were obtained by either cooling down or heating up the model at $T=500$ K. Figures 4–6 demonstrate that there are no systematic differences between data obtained for $N=2000$ and $N=5000$ series.

Figures 4 and 5 also show the atomic volume and energy of the fcc phase, which is the most stable for the EA potential at low temperatures. In order to obtain these data, we used a model consisting of 2000 atoms. First we determined the equilibrium lattice parameter at $T=0$. Then we increased the temperature by 100 K, found new equilibrium lattice parameter and ran MD at equilibrium lattice parameter for 20 000 MD steps to get equilibrium fcc properties. Then the temperature was increased by another 100 K and so on until we reached 1100 K. While this last temperature is above the melting temperature, it is not surprising that the fcc phase can be considerably overheated. The point is that in this simulation the model does not contain any crystal defects and only homogeneous nucleation of the liquid phase is possible. Figures 4 and 5 clearly demonstrate that the properties of the γ phase are different from those of the fcc phase.

B. Comparison of properties of low and high temperature noncrystalline phases

The results of the simulations described above show that two different noncrystalline phases exist at the same temperature in the single-component system described by the EA potential.[35] In this section, we explore the difference between these two phases. We will compare both phases at $T=700$ K. Figure 8 shows snapshots of the atomic positions for both phases. We could not find any obvious visual difference in the structures of these phases. Figure 9 shows the pair correlation functions of the two phases. They differ considerably in the region of the second and third peaks. In particular, the second peak of the γ phase exhibits a splitting, which is typical for an amorphous phase. This difference cannot be attributed to the difference in the atomic density ($\sim 3\%$ at $T=700$ K). Indeed, the PCF of the liquid calculated at $T=700$ K and at the density of the γ phase (the pressure is 1.4 GPa) shown in Fig. 9 is only slightly different from the PCF of the liquid at the equilibrium liquid density. Figure 9 also shows the PCF of the fcc at the same temperature, which is very different from the PCFs of the disordered phases.

Figure 10 shows the angle distributions within the first, second, and third coordination spheres (the same radii of spheres, taken from the PCF of the γ phase, were used for all phases—see the figure caption for details). Figure 10(a) demonstrates that the angle distribution only weakly depends on the density. Therefore, we will use the angle distribution of

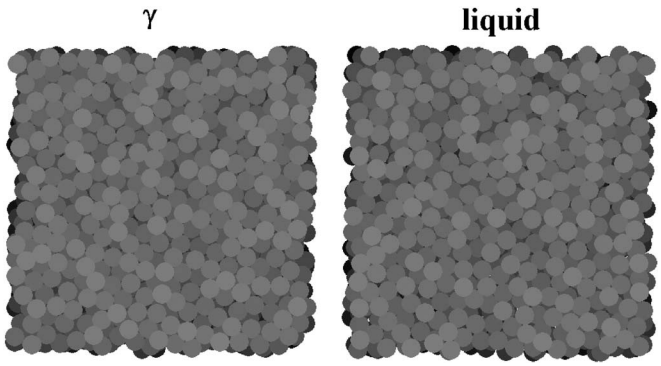

FIG. 8. Snapshots of the liquid and γ phases at $T=700$ K.

the liquid taken at the equilibrium γ-phase density [Figs. 10(b)–10(d)]. In the first coordination sphere, the only difference between the liquid and γ phases is that the angle distribution for the γ phase is sharper. Similar to the PCFs, this difference cannot be attributed to the difference in the atomic density. On the other hand, the angle distributions for the fcc and hcp phases have quite different character than those for the disordered phases. It is especially important that the peaks at 90°, 120°, and 180° [Fig. 10(b)] are absent in the distributions of the disordered phases. Surprisingly, in spite of the intuitive idea about the absence of the long distance correlations in disordered phases, the most pronounced difference between the liquid and γ phases is observed in the third coordination sphere [Fig. 10(d)]. The angle distribution for the γ phase demonstrates peaks at 120°, 150°, and 180°, which are absent in the distribution of the liquid. It is interesting to note that these peaks are typical for the distributions for the fcc and hcp phases while Fig. 10(b) clearly demonstrates that the γ phase is neither fcc nor hcp. The difference between the angle distribution in the second coordination sphere [Fig. 10(c)] in the liquid and γ phases is intermediate

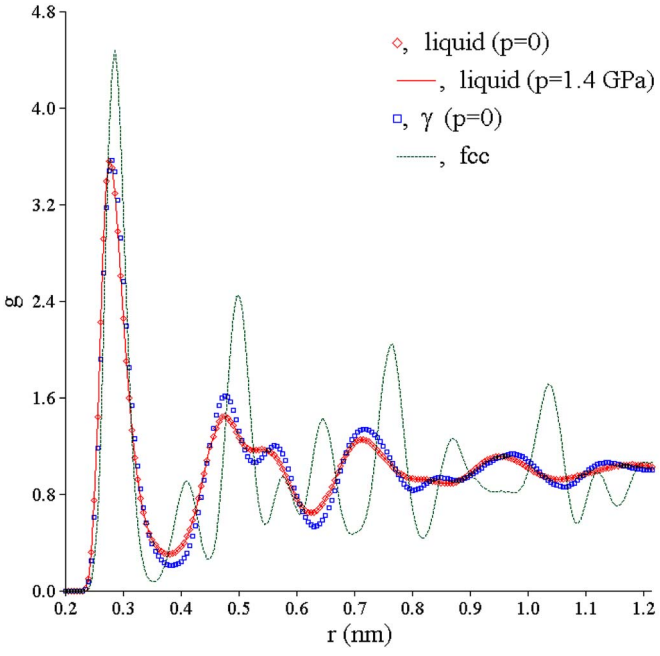

FIG. 9. (Color online) PCFs at $T=700$ K.

between those of the first and third coordination spheres. Overall, this structure analysis shows that the liquid and γ phases are similar with some noticeable differences in the second and third coordination spheres. On the other hand, we found important difference of these phase structures from the fcc and hcp phases.

Figure 11 clearly shows that the liquid and γ phases have different equations of state. Expanded by 4%, the γ phase transformed into the liquid and the corresponding point appeared on the curve for the liquid. By analogy, we should expect that under strong compression, the liquid should transform into the γ phase. Figure 11 shows that in this case the situation is more complicated. Indeed, we see the phase transformation in the liquid compressed by 5% and 6%. However, while the point corresponding to the 6% compression falls onto the γ-phase curve, the point corresponding to the 5% compression (shown as small diamond) does not. The visual analysis of the models shows that in the case of 5%, we occasionally obtained some crystalline phase. Figure 12 shows that this phase indeed has a rather low energy and Fig. 13 demonstrates that this structure has a diffusivity which is smaller than we could expect based on the curve for the γ phase. We also took the model compressed by 6% and expanded it in order to get a new model corresponding to the 5% compression. The points corresponding to this new model fall on the γ-phase curves. Overall, the data presented in Figs. 11–13 show that the liquid and γ phases have essentially different thermodynamic and kinetic properties. They also demonstrate that the properties of the low temperature noncrystalline phase (γ) are well reproducible since we obtained almost the same results for the models obtained by heating of the γ-phase model relaxed at $T=300$ K and by compressing of the liquid model at $T=700$ K.

For further investigation of the difference between the two disordered phases, we focused on the study of diffusion. First, we took the γ-phase model at $T=700$ K and equilibrium density and calculated the displacements of all atoms from their initial positions. The number of atoms with the displacement within the interval from r to $r+dr$ is proportional to dr and the number of atoms in the simulation cell,

$$dN = G_s(r,t)Ndr, \tag{4}$$

where $G_s(r,t)$ is the van Hove self-correlation function

$$G_s(r,t) = \frac{1}{N}\sum_{i=1}^{N} \delta(|\mathbf{r}_i(t) - \mathbf{r}_i(0)| - r),$$

which depends on the character of the diffusion in the system under investigation. This distribution function is shown in Fig. 14. The analysis of this plot shows that most atoms do not diffuse but rather vibrate near their equilibrium positions. It is interesting to note the presence of a very distinct second peak of this distribution, which indicates that there is a preferable diffusion jump distance in the system. Such a feature is typical for the vacancy mechanism of diffusion in crystals.[43] With time, the height of the first (vibrational) peak decreases and the height of the second (diffusional) peak

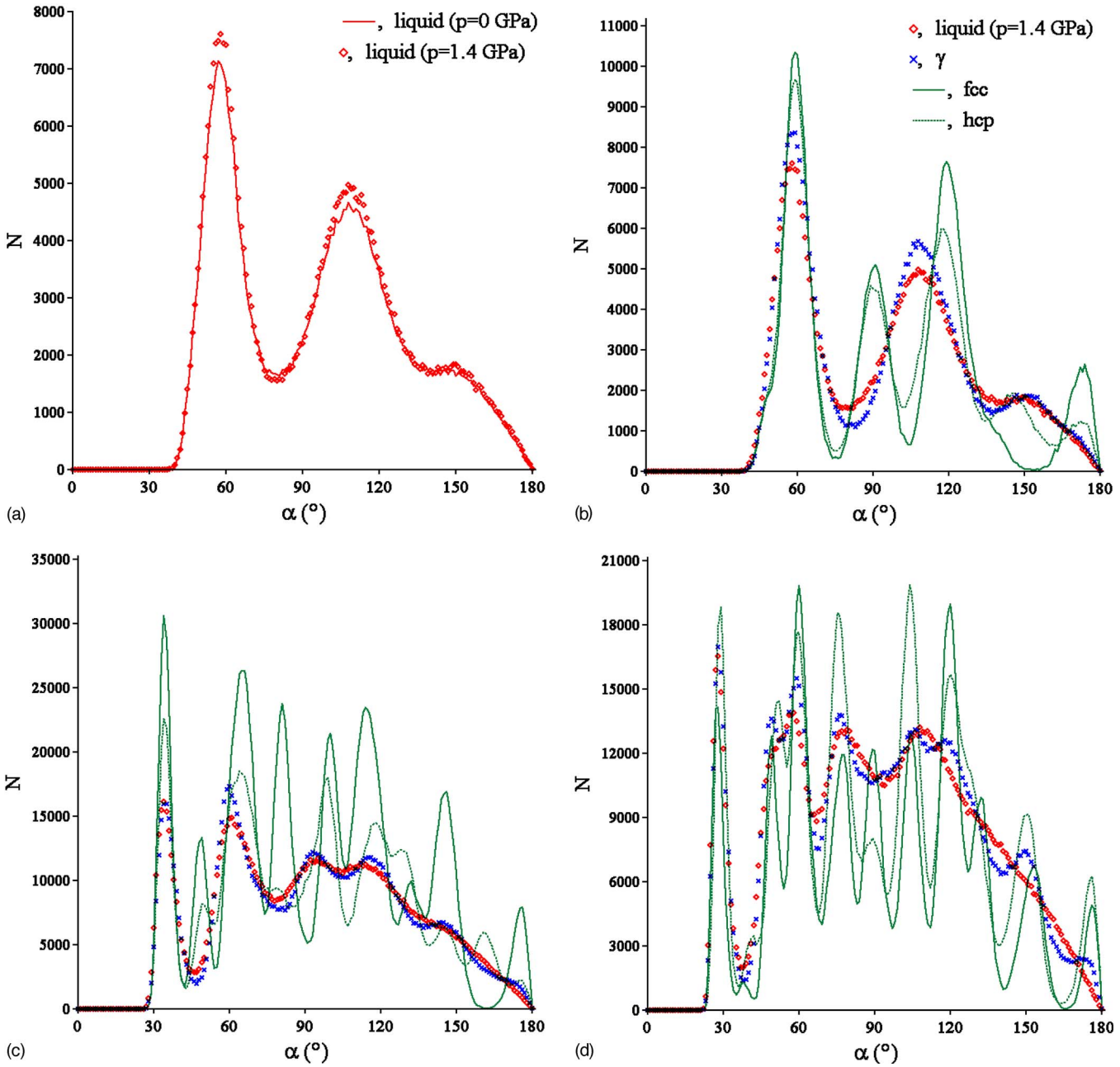

FIG. 10. (Color online) Angle distributions at $T=700$ K; in (a) and (b) the first coordination sphere (from 0 to 0.38 nm), in (c) the second coordination sphere (from 0.38 to 0.53 nm), and (d) in the third coordination sphere (from 0.53 to 0.63 nm). The radii are taken from the PCF of the γ phase.

increases but their coordinates remain the same. The same behavior of the van Hove self-correlation function was observed in Ref. 24 for the two-component amorphous Lennard-Jones system. Figure 14 also shows the displacement distribution for the liquid calculated at the same temperature and density (at a pressure of 1.4 GPa). It has quite different character: there is only one peak for this distribution and its coordinate moves to larger displacements with time. Figure 14 clearly demonstrates that the diffusion mechanisms are fundamentally different in these two disordered phases.

IV. SIMULATION OF COEXISTENCE OF LOW AND HIGH TEMPERATURE NONCRYSTALLINE PHASES

A. Determination of the coexistence temperature

The analysis made in the previous section demonstrates that in the system described by the EAM potential from Ref. 35, two different noncrystalline phases can exist as metastable phases in a wide temperature interval. We now investigate the type of the transition between these two phases. First we recall that at $T=550$ K we saw a spontaneous transformation of the liquid into the γ phase. This indicates that the transition temperature is above 550 K.

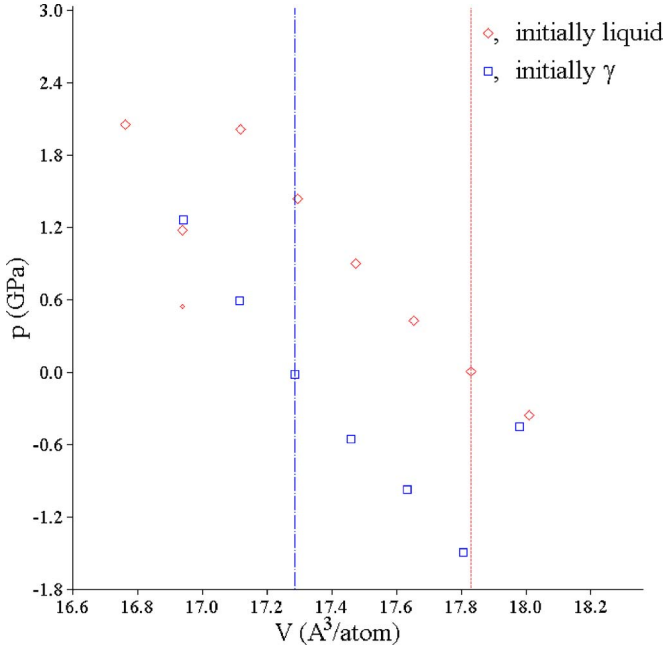

FIG. 11. (Color online) p-V diagrams at $T=700$ K.

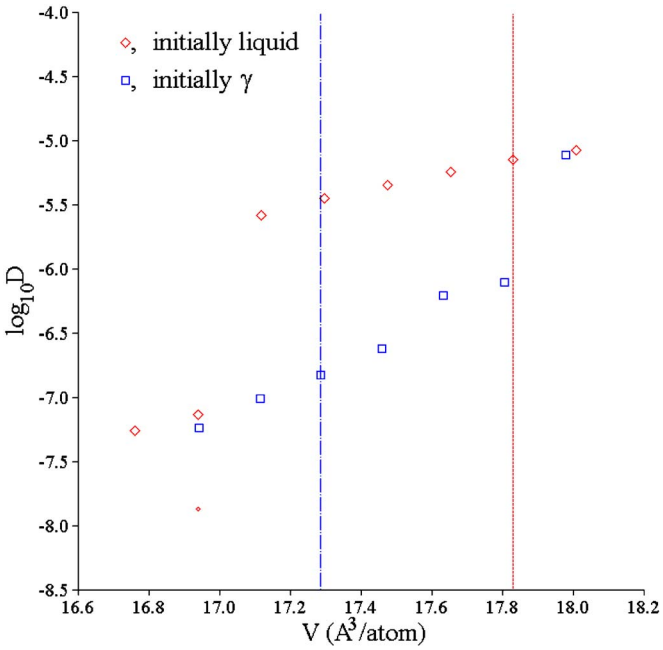

FIG. 13. (Color online) Diffusivity vs volume at $T=700$ K.

The fact that the two phases have different energies versus temperature, as shown in Fig. 5, suggests that the transition is of the first order with a latent heat. Therefore, an interface must be present if two phases coexist. In order to check this assumption, we took the γ-phase model consisting of 5000 atoms at $T=700$ K and equilibrium density and translated it four times in the z direction such that the final model contained 25 000 atoms and its extension in the z direction was five times larger than in the x and y directions. Next, we heated the upper half of the model up to 1000 K and cooled the bottom half down to 300 K. At the same time, we changed the model size in the z direction to account for the difference in the atomic densities of the liquid and γ phases (see Fig. 4). Then, we performed NVT MD simulation for 0.04 ns at $T=700$ K (model #1) and at $T=750$ K (model #2). Finally, we performed NVE (i.e., N=const, V=const, and E=const) simulations for 4 ns.

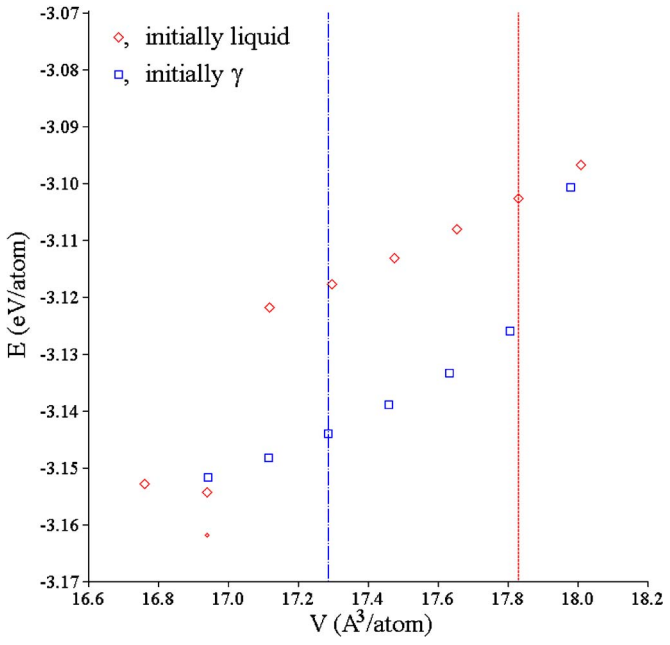

FIG. 12. (Color online) Energy vs volume at $T=700$ K.

Figure 15 shows the evolution of the temperature and pressure during this simulation; roughly, these quantities converge after about 2 ns (half of the total simulation time). This demonstrates that the simulation time was definitely enough to equilibrate the simulation cell. A snapshot of model #1 is shown in Fig. 16. While it is difficult to see any interface on this snapshot, the energy distribution plot clearly demonstrates that there are two such interfaces in the simulation cell (recall that it has periodic boundary conditions in the z direction). The comparison with Fig. 5 shows that one region of the simulation cell has an energy typical for the γ phase and another region has an energy typical for the liquid. The diffusivity in the liquid region is one order of magnitude higher than in the γ-phase region (see Fig. 16). Thus, we conclude that after the long NVE simulation we still have two phases in the simulation cell. Therefore, the final temperature (722 K) in the simulation cell is the phase transformation temperature at the final pressure (−0.19 GPa). In the case of first-order transformation between these two phases, the transition temperature at zero pressure can be calculated using the Clausius-Clapeyron equation,

$$\frac{dp}{dT} = \frac{\Delta E}{T\Delta V}, \tag{5}$$

and the data from Figs. 4 and 5. Using the data obtained from model #1, we find that the $\gamma \rightarrow$ liquid transformation temperature is 733 K. For the model #2, we obtained that the final temperature is 748 K at the final pressure $p=0.12$ GPa, and, therefore, the transition temperature is 740 K. It is not

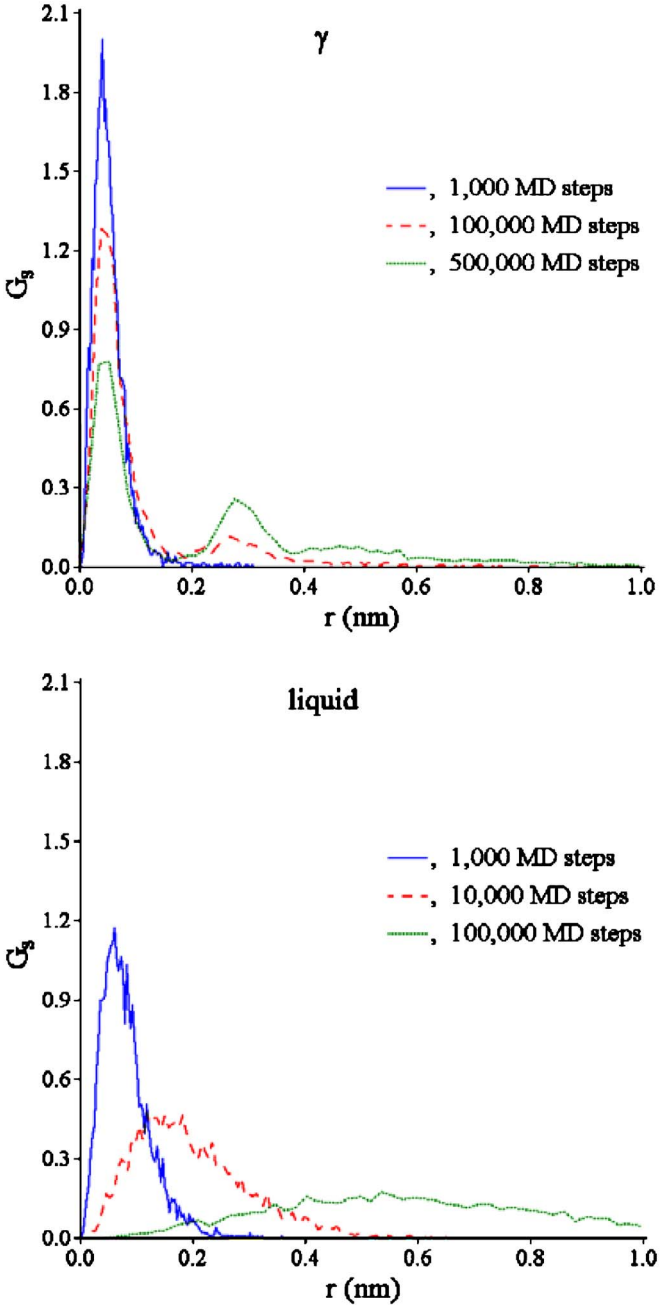

FIG. 14. (Color online) The van Hove self-correlation functions of the liquid and γ phases at $T=700$ K and the density equal to the equilibrium density of the γ phase.

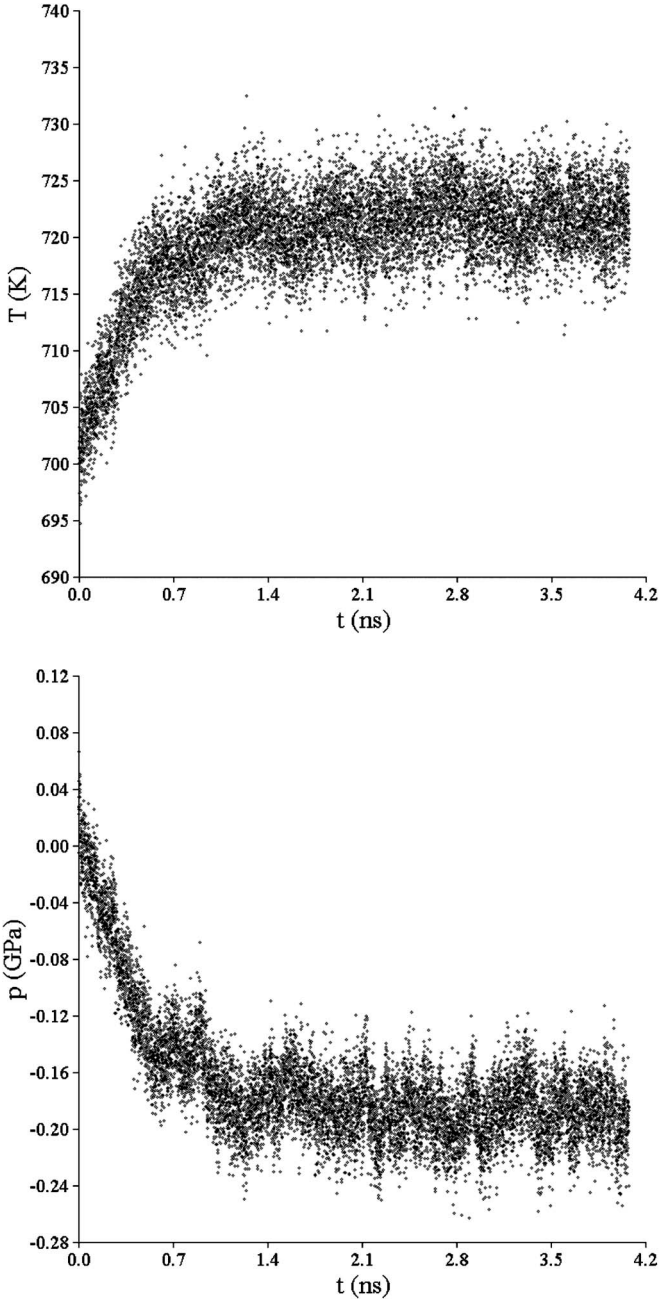

FIG. 15. Time dependences of the temperature and pressure in the NVE simulation of the liquid and γ phase coexistence.

clear why the two simulations gave slightly different results for the transition temperature.

B. Simulation of low-high temperature noncrystalline phases interface migration

One could argue that the reason that the simulation cell contained two phases after the MD relaxation during 2 000 000 steps (4 ns) is associated with the fact that this time was not enough to establish local equilibrium. This could be the case if the interface mobility is very small. Therefore, we performed additional simulations to obtain this quantity. We used model #2 from the previous section and cut it normally to the z direction in the middle of the liquid region. Then we converted the dividing plane into two free surfaces such that we had γ-phase region in the middle simulation cell and two liquid regions on the edges. We changed the simulation cell size in order to get the equilibrium γ-phase density at $T=780$ K (using data shown in Fig. 4) and made 20 000 MD steps at $T=780$ K.

The total energy distribution in this model (#I0), shown in Fig. 17, clearly demonstrates that the simulation cell consists of three regions: two liquid regions and one γ-phase regions. Next, we relaxed the simulation during 520 000 MD steps at $T=780$ K. We refer the final model as #I1. Since the simu-

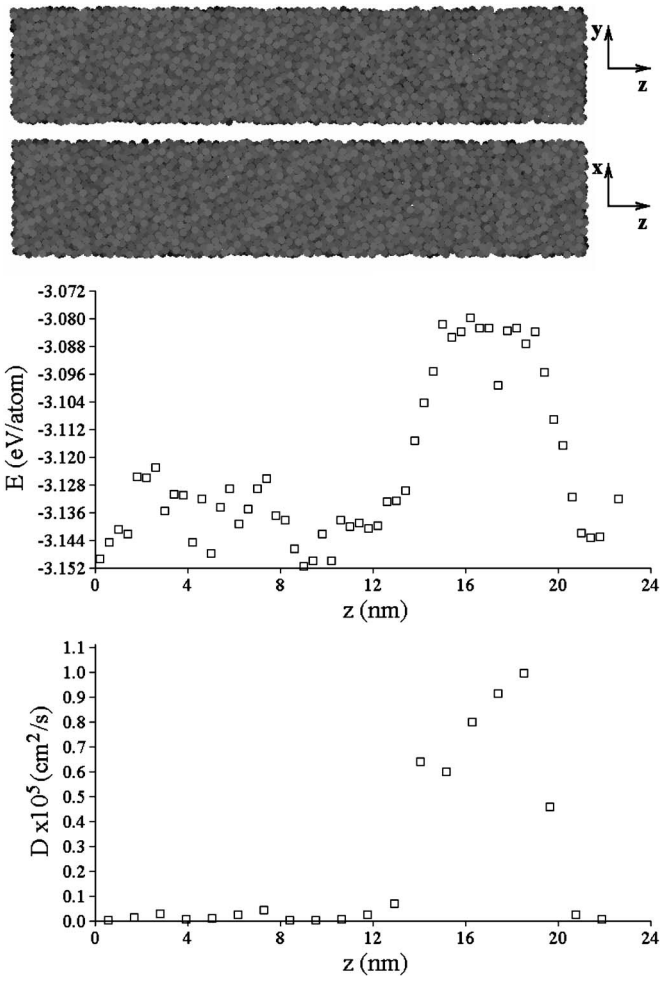

FIG. 16. (Top) Snapshot of the simulation cell containing the γ phase in the lower z part (left side of figure) and the liquid in the upper z part. Also shown are (middle) energy and (bottom) diffusivity distributions in z.

lation temperature, $T=780$ K, was above the transition temperature, the liquid was supposed to grow at the expense of the γ phase. Indeed, Fig. 17 shows that the γ phase shrunk to the narrow layer in the middle of the simulation cell. Since the energy of the liquid is higher than that of the γ phase, the total energy was supposed to increase, as indeed can be seen from Fig. 18. The interface velocity was determined as

$$V = \frac{1}{2L_x L_y n_\gamma \Delta E_{\gamma\to\text{liquid}}} \frac{dE}{dt}, \tag{6}$$

where L_x and L_y are the simulation cell sizes in the x and y directions, n_γ is the γ-phase atomic density, $\Delta E_{\gamma\to\text{liquid}}$ is the energy of the $\gamma\to$liquid transformation and factor 2 accounts for the presence of the two interfaces in the simulation cell.

Next, we set the temperature to $T=700$ K and changed the simulation cell size according to the data presented in Fig. 4. During the MD relaxation at $T=700$ K, the total energy decreased (see Fig. 18), indicating that the γ phase grew in this simulation at the expense of the liquid. This can be also seen from the total energy distribution in the final configuration (#I2) shown in Fig. 17. We repeated this procedure of MD relaxation at $T=700$ K and $T=780$ K several times (see Fig. 17), obtaining additional models #I3, #I4, and #I5. The interface velocity was determined in each simulation and the results are shown in Fig. 19. If we assume a linear velocity-driving force relationship and assume that the driving force is proportional to $T-T_{\gamma\to\text{liquid}}$, we can obtain from this plot the transition temperature and the kinetic coefficient defined as

$$V = \mu(T - T_{\gamma\to\text{liquid}}). \tag{7}$$

The kinetic coefficient was found to be equal to 0.21 m/(s K). The transition temperature was found to be equal to $T_{\gamma\to\text{liquid}}=752$ K. This value is a little higher than that found in the previous section and is probably associated with the fact that we obtained the γ-phase structure with lower energy when it slowly grew from the liquid than the γ phase which we originally obtained from the model relaxed at much lower temperature ($T=300$ K).

In order to confirm this transition temperature, we took model #I4, relaxed it at $T=780$ K during 300 000 MD steps (in order to let the interfaces make the half distance to the simulation cell edges) and then switched to NVE simulation. This simulation shows that the transition temperature is 757 K, which is in reasonable agreement with the results of the moving interface simulation. A snapshot of model #I4 is shown in Fig. 17. While some elements of fourfold symmetry can been seen in planes which are normal to the y direction, they do not extend over the entire simulation cell. No signs of symmetry are seen in planes which are normal to the x direction. In addition, the analysis of the angle distribution, similar to that presented in Fig. 10, did not reveal any sign of crystallinity.

The fact that the interface could be driven in either direction by over- or undercooling demonstrates that the presence of this interface during longtime coexistence simulations cannot be explained by insufficient simulation time. In fact, the relaxation of the temperature and pressure shown in Fig. 15 is due to interface motion, showing that the interface can move in this time frame, and come to equilibrium during the simulations.

V. THE KAUZMANN TEMPERATURE

An important quantity for the thermodynamic characterization of a supercooled liquid is the Kauzmann temperature T_K, which is a consequence of the difference in the liquid and crystal heat capacities.[44] Since at the melting temperature, the entropy of the liquid, S_L is larger than that of the crystal, S_C, the different slope of their temperature dependences implies that their difference,

$$\Delta S(T) = S_L(T) - S_C(T) = \frac{\Delta E(T)}{T} - \int_T^{T_m} \frac{\Delta E(T')}{T'^2} dT', \tag{8}$$

decreases with decreasing temperature and eventually vanishes proportionally to $(T-T_K)$ at the Kauzmann temperature T_K. While there is no thermodynamic principle that requires $\Delta S>0$, it has been proposed that an ideal glass transition takes place at T_K.[45] Then the system is expected to be in one

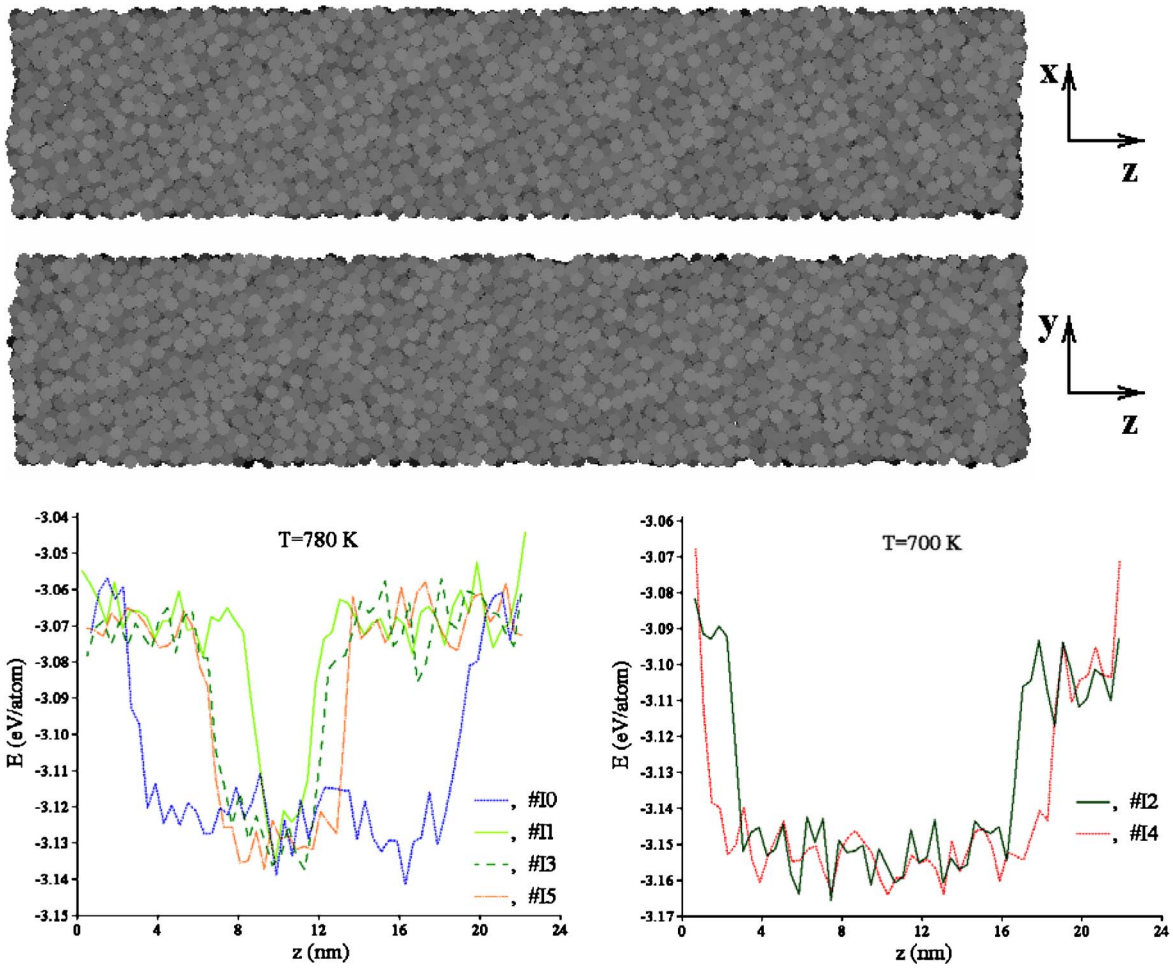

FIG. 17. (Color online) Snapshot of model #I4 and total energy distributions in models #I0-I5.

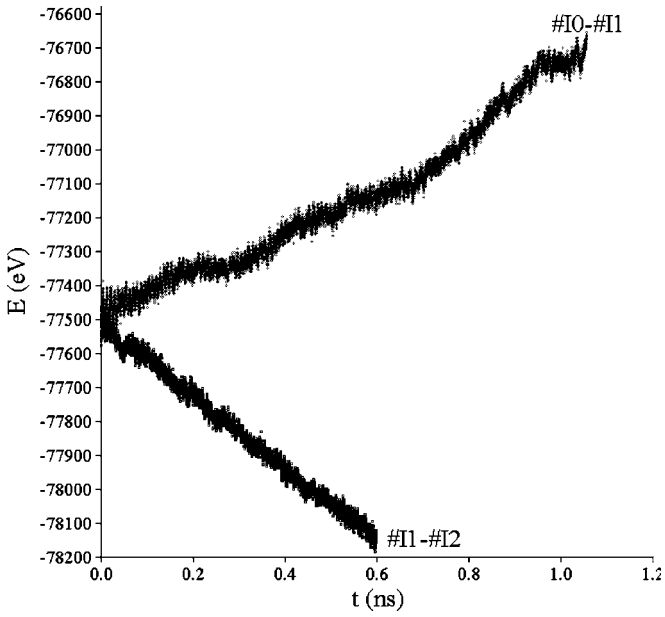

FIG. 18. Total energy vs time in the NVT simulations producing the models I1 and I2.

of the few lowest amorphous potential energy minima. While T_K is inaccessible experimentally due to the fact that the supercooled liquid will fall out of equilibrium at higher temperatures, it has served as an important theoretical concept.[46] Most notably is the agreement between the value for T_K and the temperature T_0 where the viscosity of a supercooled liquid diverges according to the Vogel-Fulcher expression,

$$\eta(T) = \eta_0 \exp[-D/(T - T_0)]. \quad (9)$$

T_0 and T_K are very close for a large number of glass-forming liquids.[47] Below $T_K \cong T_0$ even slow activated dynamics of the supercooled liquid are arrested.

We can estimate the Kauzmann temperature directly from Eq. (8), since T_m and $\Delta E(T)$ can be obtained from the MD simulation. The calculation of $\Delta E(T)$ is straightforward and the melting temperature in the present work was obtained using the coexistence method proposed in Ref. 48. We found T_m=925 K and T_K=317 K. As was expected, the Kauzmann temperature is below the transition temperature found in the previous section.

We can also perform the analysis replacing the crystal internal energy by that of the γ phase and the melting temperature by the transition temperature found in the previous section. We found that T_K'=425 K, which is higher than the

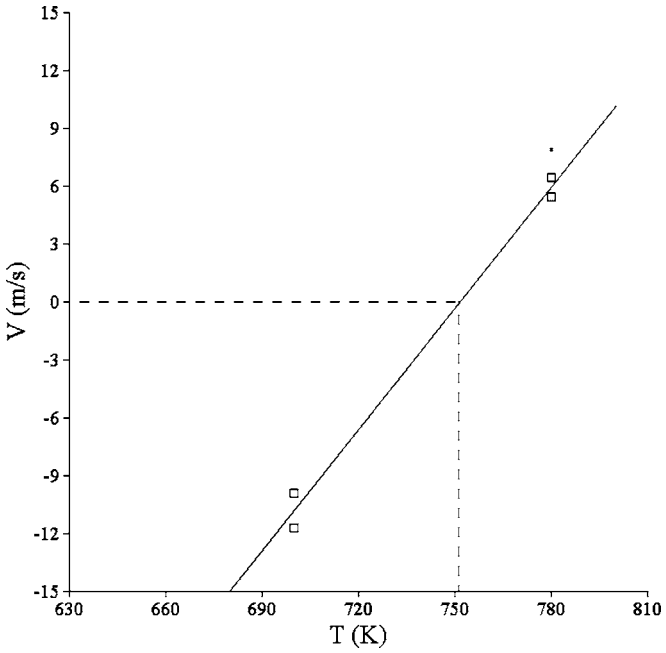

FIG. 19. The interface velocity vs temperature. The small square corresponding to model #I1 was excluded from the calculation of the kinetic coefficient.

value obtained for the fcc phase. This is a consequence of the fact that the entropy of γ phase is larger than that of the fcc phase. It is important to note that even this new Kauzmann temperature is below the transition temperature found in the previous section.

VI. DISCUSSION

In this paper we present the results of extensive molecular dynamics simulations of liquid structure and dynamics in the one-component system described by the Ercolessi-Adams EAM potential for Al. We never observed crystallization in this system, consistent with our previous work where we found that this potential predicts a rather high solid-liquid interface free energy.[38] Instead, we found two distinct noncrystalline phases in the system. One of them is a liquid phase. The second phase (γ) has a rather similar structure (by several common measures) but definitely a different equation of state: it is both lower in potential energy and higher in density at coexistence. Moreover, this phase has qualitatively different dynamics than that of the liquid. First, the diffusivities in the liquid and γ phases are different by at least one order of magnitude even if both phases are at the same density and temperature. Second, the van Hove self-correlation function for the liquid has only one maximum which shifts to the larger distances with time as expected for ordinary diffusion in liquids. In contrast, the van Hove function of the γ phase has several peaks. The first peak corresponds to the vibrational motion of most atoms near their equilibrium position. The position of this peak does not change with time. The second peak corresponds to diffusion jumps. This is very similar to the behavior of the van Hove function observed in Ref. 24 for binary Lennard-Jones system known to be glass forming.

We found that there is a temperature interval where both noncrystalline phases are metastable, exhibiting no transition over molecular dynamics time scales. This interval is above the Kauzmann temperature where the entropy of the liquid phase is equal to that of the fcc phase. This is also consistent with the observations for the glass transition made in Ref. 22. Therefore, the EA potential gives us an opportunity to investigate the glass formation and structure evolution in a single-component system.

Both $\gamma \rightarrow$ liquid and liquid $\rightarrow \gamma$ transitions can be seen during MD simulations (see Fig. 7). If these phases can coexist, the coexistence temperature should be between the temperatures where we observe these transitions. The hysteresis, the distinct energy, and density behaviors of the different phases shown in Fig. 5, and the discontinuous transitions shown in Fig. 7, motivated our study of the coexistence of these two noncrystalline phases. We found that the interface between these two phases does not disappear during MD simulation. Instead, the coexisting system evolves toward a pressure and temperature where there is no driving force for interface motion: namely, where the two free energies are identical. This determines the coexistence temperature in the exactly the same manner as has been done for the melting temperature. We found that above the coexistence temperature, the interface moves toward the γ phase. Similarly, below the coexistence temperature, it moves toward to the liquid. This observation demonstrates that the coexistence simulation times are sufficiently long to allow the interface to migrate out of the system if there were any significant driving force. The presence of the interface also supports the conclusion that the transformation is of the first order. We also found the mobility of this interface, which appeared to be about two times smaller than the solid-liquid interface mobility in the same system.[49]

The bulk properties of the glass phase were obtained using the NVT simulation (Figs. 4, 6, and 9–14). A concern could be that the observation of this phase is due to constraints imposed by the NVT scheme. However, some of our coexistence simulations (Sec. IV B) were performed with two free surfaces in the z direction. Obviously, the volume of each subsystem is allowed to change in this scheme. Finally, the fact that the low temperature noncrystalline phase is stable with respect to liquid at low temperature follows from the fact that the interface between these two phases moves toward to liquid at low temperatures.

The transformation between two noncrystalline phases found above is rather different from the one expected for usual vitrification,[50,51] where the free energy of the glass is larger than the equilibrium free energy of the liquid state by TS_c, where S_c is the configurational entropy of order $\Delta S(T)$ in Eq. (8). In other words, this model suggests that in our case,[18]

$$F_\gamma = F_{\text{liquid}} + TS_c. \tag{10}$$

However, this is in contradiction with our simulation results. Indeed, below the coexistence temperature, the interface moves toward to the liquid, demonstrating that the γ phase has lower free energy. Of course, Eq. (10) for F_γ is based on the assumption that no aging effect occurs in the glass

state.[19] Such effects may lead to a nucleationlike dynamics as seen in our simulation.[52]

Our simulation results could be also consistent with a picture where there are two competing liquid states, one of which is already vitrified. This would be similar to the first-order glass-to-liquid transition in Si, with an underlying liquid-liquid transition, as seen in flash-heating experiments[53] and computer simulations.[54] These results strongly suggest that supercooled liquids should not be considered as homogeneous but that there exist multiple locally favored structures. A scenario that is consistent with our simulation results would be the existence of an equilibrium liquid-liquid transition located below the glass temperature for the liquid phase, which is more stable at low temperatures. Finally, a third possibility to explain our results would be the assumption that the γ phase is a highly defective crystal (or possibly quasicrystal) phase which we could not identify.

VII. SUMMARY

We presented the results of molecular dynamics study of the liquid structure and dynamics in the one-component system described by the Ercolessi-Adams EAM potential. We found two distinct noncrystalline phases in this system. One of them is a liquid phase and the second phase has similar structure but definitely different equation of state. Moreover, this phase has qualitatively different dynamics than that in the liquid phase. The transitions between these two noncrystalline phases can be seen during MD simulation. We found the coexistence temperature and the interface mobility. The presence of the interface and nonzero latent heat show that the transformation is of the first order.

ACKNOWLEDGMENTS

The authors thank G. J. Ackland, Rachel S. Aga, B. S. Bokstein, J. W. Cahn, M. J. Kramer, H. Sheng, J. A. Warren, and P. G. Wolynes for helpful discussions. The Ames Laboratory is operated by the U.S. Department of Energy (DOE) by Iowa State University under Contract No. W-7405-ENG-82. This work was supported by the Office of Basic Energy Sciences. J.R.M. acknowledges the support of the Division of Materials Sciences and Engineering, Office of Basic Energy Sciences, U.S. Department of Energy under Contract No. DE-AC05-000R-22725 with UT-Battelle. We acknowledge partial funding from DOE's Computational Materials Science Network project, "Microstructural Evolution Based on Fundamental Interfacial Properties," and computer time from the National Energy Research Scientific Computing Center.

[1] W. L. Johnson, Mater. Res. Bull. **11**, 104 (1999).
[2] A. Inoue, in *Bulk Amorphous Alloys* (Trans Tech Publications, Zurich, 1998).
[3] F. C. Frank and J. S. Kaspar, Acta Crystallogr. **12**, 483 (1959).
[4] R. W. Cahn, in *Materials Science and Technology*, edited by R. W. Cahn, P. Hanssen, and E. J. Kramer (VCH, Weinberg, 1991), p. 403.
[5] D. Shechtman, I. Blech, D. Gratias, and J. W. Cahn, Phys. Rev. Lett. **53**, 1951 (1984).
[6] A. Inoue, Acta Mater. **48**, 279 (2000).
[7] S. Sachdev and D. R. Nelson, Phys. Rev. Lett. **53**, 1947 (1984).
[8] P. H. Poole, T. Grande, C. A. Angell, and P. F. McMillan, Science **275**, 322 (1997).
[9] O. Mishima and H. E. Stanley, Nature **396**, 329 (1998).
[10] F. Sciortino, J. Phys.: Condens. Matter **17**, 7 (2005).
[11] C. Z. Wang and K. M. Ho (private communication).
[12] Y. Singh, J. P. Stoessel, and P. G. Wolynes, Phys. Rev. Lett. **54**, 1059 (1985).
[13] X. Xia and P. G. Wolynes, Proc. Natl. Acad. Sci. U.S.A. **97**, 2990 (2000).
[14] W. Kob and H. C. Andersen, Phys. Rev. E **52**, 4134 (1995).
[15] W. Kob and H. C. Andersen, Phys. Rev. Lett. **73**, 1376 (1994).
[16] T. R. Kirkpatrick, D. Thirumalai, and P. G. Wolynes, Phys. Rev. A **40**, 1045 (1989).
[17] W. Gotze and L. Sjogren, Rep. Prog. Phys. **55**, 241 (1992).
[18] M. Mezard and G. Parisi, J. Chem. Phys. **111**, 1076 (1999).
[19] L. F. Cugliandolo and J. Kurchan, Philos. Mag. B **71**, 501 (1995).
[20] W. Kob and J.-L. Barrat, Phys. Rev. Lett. **78**, 4581 (1997).
[21] W. Kob, F. Sciortino, and R. Tartaglia, Europhys. Lett. **49**, 590 (2000).
[22] S. Sastry, Nature **409**, 164 (2001).
[23] G. Adam and J. H. Gibbs, J. Chem. Phys. **43**, 139 (1965).
[24] S. Sastry, P. G. Debenedetti, and F. Stillinger, Nature **393**, 554 (1998).
[25] R. N. Barnett, C. L. Cleveland, and U. Landman, Phys. Rev. Lett. **55**, 2035 (1985).
[26] Y. Qi, T. Cagin, Y. Kimura, and William A. Goddard III, Phys. Rev. B **59**, 3527 (1999).
[27] G. Duan, D. Xu, Q. Zhang, G. Zhang, T. Cagin, W. L. Johnson, and William A. Goddard III, Phys. Rev. B **71**, 224208 (2005).
[28] L. Wang, X. Bian, and J. Zhang, J. Phys. B **35**, 3575 (2002).
[29] H. R. Cong, X. F. Bian, J. X. Zhang, and H. Li, Mater. Sci. Eng., A **326**, 343 (2002).
[30] L. Wang, X. F. Bian, and H. Li, Mater. Lett. **51**, 7 (2001).
[31] H. Teichler, Phys. Rev. Lett. **76**, 62 (1996).
[32] H. Pang, Z. H. Jin, and K. Lu, Phys. Rev. B **67**, 094113 (2003).
[33] M. S. Daw and M. I. Baskes, Phys. Rev. B **29**, 6443 (1984).
[34] F. Ercolessi and J. B. Adams, Europhys. Lett. **26**, 583 (1994).
[35] X.-Y. Liu, P. P. Ohotnicky, J. B. Adams, C. Lane Rohrer, and R. W. Hyland, Surf. Sci. **373**, 357 (1997).
[36] M. I. Mendelev, D. J. Srolovitz, G. J. Ackland, and S. Han, J. Mater. Res. **20**, 208 (2005).
[37] R. S. Aga, J. R. Morris, J. J. Hoyt, and M. Mendelev, Phys. Rev. Lett. **96**, 245701 (2006).
[38] J. R. Morris, M. I. Mendelev, and D. J. Srolovitz, J. Non-Cryst. Solids (to be published).
[39] C. S. Liu, Z. G. Zhu, J. Xia, and D. Y. Sun, J. Phys.: Condens. Matter **13**, 1873 (2001).

[40] G. X. Li, Y. F. Liang, Z. G. Zhu, and C. S. Liu, J. Phys.: Condens. Matter **15**, 2259 (2003).
[41] W. G. Hoover, *Molecular Dynamics* (Springer-Verlag, New York, 1986).
[42] Y. Waseda, *The Structure of Non-crystalline Materials* (McGraw-Hill International Book Co., New York, 1980).
[43] P. G. Shewmon, *Diffusion in Solids* (McGraw-Hill, New York, 1963).
[44] W. Kauzmann, Chem. Rev. (Washington, D.C.) **43**, 219 (1948).
[45] C. A. Angell and J. C. Tucker, J. Phys. Chem. **78**, 278 (1974).
[46] J. H. Gibbs and E. A. DiMarzio, J. Chem. Phys. **28**, 373 (1958); G. Adam and J. H. Gibbs, *ibid.* **43**, 139 (1965).
[47] P. G. Debenedetti, *Metastable Liquids, Concepts and Principles* (Princeton University Press, Princeton, NJ, 1996).
[48] J. R. Morris, C. Z. Wang, K. M. Ho, and C. T. Chan, Phys. Rev. B **49**, 3109 (1994).
[49] J. J. Hoyt (private communication).
[50] P. G. Debenedetti and F. Stillinger, Nature **410**, 259 (2001).
[51] C. A. Angel, Science **267**, 1924 (1995).
[52] V. Lubchenko and P. G. Wolynes, J. Chem. Phys. **121**, 2852 (2004).
[53] E. P. Donovan, F. Saepen, D. Turnbull, J. M. Poate, and D. C. Jacobson, J. Appl. Phys. **57**, 1795 (1985).
[54] W. D. Luedtke and U. Landman, Phys. Rev. B **37**, 4656 (1988).